

## Effects of variable viscosity and thermal conductivity on magnetohydrodynamic free convection dusty fluid along a vertical porous plate with heat generation

Gopal Chandra HAZARIKA<sup>1,\*</sup>, Jadav KONCH<sup>1,2</sup>

<sup>1</sup>Department of Mathematics, Faculty of Mathematics, Dibrugarh University, Dibrugarh, India

<sup>2</sup>Department of Mathematics, Research Scholar of Mathematics, Dibrugarh University, Dibrugarh, India

Received: 12.09.2015

Accepted/Published Online: 19.01.2016

Final Version: 12.02.2016

**Abstract:** The present study investigated the effects of variable viscosity and thermal conductivity on a two-dimensional steady laminar magnetohydrodynamic (MHD) free convective boundary layer flow of a dusty fluid over a vertical porous flat plate with viscous dissipation, Joule heating, and heat generation/absorption. Governing partial differential equations of motion were reduced to a system of ordinary differential equations using similarity transformations. The resulting boundary value problem was then solved numerically using the shooting technique. Velocity, temperature, and species concentration profiles of fluid and solid particles were obtained for different flow governing parameters. The results are presented in graphs. We found that viscosity and species concentration decrease and temperature increases with the increasing value of the viscosity variation parameter for both the fluid and dust particles. Quite the opposite phenomenon was seen with the thermal conductivity variation parameter. Finally, the skin friction coefficient, Nusselt number, and Sherwood number are presented in tables for various flow governing parameters.

**Key words:** Dusty fluid, variable viscosity and thermal conductivity, viscous dissipation, Joule heating

### 1. Introduction

Dusty fluid flows are concerned with the motion of liquid or gas containing immiscible inert solid particles. Common examples of dusty fluid systems include blood flow in arteries, flows in rocket tubes, gas cooling systems to enhance the heat transfer process, movement of inert solid particles in the atmosphere and other suspended particles in seas and oceans.

Flow of dusty and electrically conducting fluid along a vertical porous plate in the presence of transverse magnetic field is very important as it has many practical applications in different areas such as applications in gas cooling systems, centrifugal separation of matter from fluid, several manufacturing processes in industries like extrusion of plastic sheets, steel manufacturing industry, glass fiber, and paper production. Moreover, it is used in metal spinning, the cooling of metallic plates in a cooling bath, polymer technology, powder technology, paint spraying, blood rheology, etc.

Thus, the study of these problems is mathematically interesting and useful for modelling the physical phenomena to address complex issues related to fluid flow characteristics.

Saffman [1] carried out pioneering work on the stability of laminar flow of a dusty gas, describing the fluid-particle system and deriving the motion of gas equations carrying the dust particles. Boundary layer flow of a dusty fluid over a semiinfinite flat plate has been analyzed by Datta and Mishra [2]. The phenomenon

\*Correspondence: gchazarika@gmail.com

of the flow of dusty fluid and heat transfer in the boundary layer has been studied by a number of authors such as Asmolov and Manuilovich [3], Palani and Ganesan [4], Agranat [5], and Vajravelu and Nayfeh [6]. Gireesha et al. [7] analyzed the boundary layer flow and heat transfer of dusty fluid over a stretching sheet with nonuniform heat source/sink. They reported that temperature-dependent heat sinks are better suited for cooling purposes. Gireesha et al. [8,9] also discussed the boundary layer flow and heat transfer of a dusty fluid over a stretching sheet with viscous dissipation for both steady and unsteady flows. Kishan and Deepa [10] analyzed the effect of viscous dissipation on stagnation point flow and heat transfer of a micropolar fluid with uniform suction/blowing. The effect of viscous dissipation on laminar mixed convection fluid in a vertical double passage channel was studied by Gaikwad and Rahuldev [11]. Investigations on the effects of variable viscosity and thermal conductivity on convective heat transfer in a dusty fluid over a vertical permeable surface with radiation and viscous dissipation were conducted by Hazarika [12].

In the aforementioned studies, the effects of physical properties were assumed as constant. However, it is known from the work of Herwig and Wicken [13] that these properties may change with temperature changes. When the effects of variable viscosity and thermal conductivity are taken into account, flow characteristics are significantly changed compared with the constant property case. In the present study an attempt was made to study the combined effects of variable viscosity and variable thermal conductivity on free convection flow of dusty fluid along a vertical porous plate embedded in a porous medium with magnetic field and heat generation. Following Lai and Kulacki [14] and Choudhury and Hazarika [15], the fluid viscosity and thermal conductivity were assumed to vary as inverse linear functions of temperature.

The governing boundary layer equations were transformed into ordinary differential equations using suitable similarity transformations. Numerical solutions of these ordinary differential equations with the prescribed boundary conditions were obtained using the fourth order Runge–Kutta shooting technique. The effects of various parameters on these solutions are discussed and illustrated through a set of figures and tables.

## 2. Mathematical analysis

Consider a steady two-dimensional laminar boundary layer flow of an incompressible viscous electrically conducting dusty fluid along a vertical stretching permeable sheet in porous medium. The sheet is coinciding with the plane  $y = 0$ , with the flow being confined to  $y > 0$ . Two equal and opposite forces are applied along the  $x$ -axis, so that the sheet is stretched, keeping the origin fixed. A transverse uniform magnetic field of strength  $B_0$  is applied in the  $y$ -direction as shown in Figure 1.

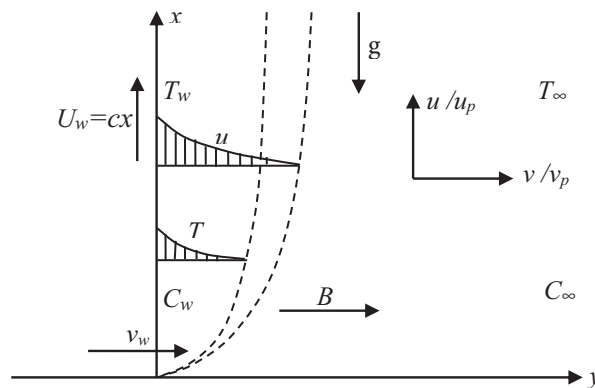


Figure 1. Schematic diagram of the flow.

The analysis is based on the following assumptions:

- Viscous dissipation, Joule heating, and heat generation are taken into account.
- Physical properties are assumed as constant except for the fluid viscosity and thermal conductivity.
- The magnetic Reynolds number is assumed to be small so that the induced magnetic field is negligible.
- Dust particles are assumed to be electrically nonconductive, spherical in shape, having the same radius and mass, and undeformable.
- The number density of dust particles is taken as constant throughout the flow.

Using the above assumptions together with the usual boundary layer approximations and following Vajravelu and Nayfeh [6], we get the equations of motion as follows:

**For the fluid phase:**

Equation of continuity:

$$\frac{\partial u}{\partial x} + \frac{\partial v}{\partial y} = 0 \quad (2.1)$$

Momentum equation:  $u \frac{\partial u}{\partial x} + v \frac{\partial u}{\partial y} = \frac{1}{\rho} \frac{\partial}{\partial y} \left( \mu \frac{\partial u}{\partial y} \right) + \frac{KN}{\rho} (u_p - u) + g\beta^*(T - T_\infty)$

$$- \frac{\sigma B_0^2}{\rho} u - \frac{\mu}{\rho k} u - \frac{c}{k} u^2 \quad (2.2)$$

Energy equation:  $\rho c_p \left( u \frac{\partial T}{\partial x} + v \frac{\partial T}{\partial y} \right) = \frac{\partial}{\partial y} \left( \lambda \frac{\partial T}{\partial y} \right) + \frac{Nc_p}{\tau_T} (T_p - T) + \frac{N}{\tau_v} (u_p - u)^2$

$$+ Q_0 (T - T_\infty) + \mu \left( \frac{\partial u}{\partial y} \right)^2 + \frac{J^2}{\sigma} \quad (2.3)$$

Species concentration equation:

$$u \frac{\partial C}{\partial x} + v \frac{\partial C}{\partial y} = \frac{\partial}{\partial y} \left( D_1 \frac{\partial C}{\partial y} \right) \quad (2.4)$$

**For the dust phase:**

Equation of continuity:

$$\frac{\partial}{\partial x} (\rho_p u_p) + \frac{\partial}{\partial y} (\rho_p v_p) = 0 \quad (2.5)$$

Momentum equations:

$$u_p \frac{\partial u_p}{\partial x} + v_p \frac{\partial u_p}{\partial y} = \frac{K}{m} (u - u_p) \quad (2.6)$$

$$u_p \frac{\partial v_p}{\partial x} + v_p \frac{\partial v_p}{\partial y} = \frac{K}{m} (v - v_p) \quad (2.7)$$

Energy equation:

$$u_p \frac{\partial T_p}{\partial x} + v_p \frac{\partial T_p}{\partial y} = - \frac{c_p}{c_m \tau_T} (T_p - T) \quad (2.8)$$

Species concentration equation:

$$u_p \frac{\partial C_p}{\partial x} + v_p \frac{\partial C_p}{\partial y} = \frac{\partial}{\partial y} \left( D_2 \frac{\partial C_p}{\partial y} \right) \quad (2.9)$$

where  $(u, v)$  and  $(u_p, v_p)$  are the velocity components of fluid and dust particle phases along the  $x$  and  $y$  directions, respectively.  $\mu, \rho, \rho_p$  and  $N$  are the coefficient of viscosity of the fluid, density of the fluid, density of the particle phase, and the number density of the particle phase, respectively.  $K$  is the Stokes' resistance (drag coefficient),  $m$  is the mass of the dust particle,  $g$  is the acceleration due to gravity, and  $\beta^*$  is the volumetric coefficient of thermal expansion.  $T$  and  $T_p$  are the temperatures of the fluid and dust particles inside the boundary layer, respectively.  $T_\infty$  and  $T_{p\infty}$  are the temperatures of fluid and dust particles in the free-stream, respectively.  $\vec{J}$  is the electric current density,  $\sigma$  is the electrical conductivity,  $k$  is the Darcy permeability constant,  $c$  is the stretching rate,  $c_p$  and  $c_m$  are the specific heats of fluid and dust particles at constant pressure, respectively,  $\tau_T$  is the thermal equilibrium time (the time required by the dust cloud to adjust its temperature to the fluid),  $\tau_v$  is the relaxation time of the dust particle (time required by a dust particle to adjust its velocity relative to the fluid),  $\lambda$  is the thermal conductivity of the fluid,  $Q_0$  is the volumetric rate of heat generation,  $C$  and  $C_p$  are the concentrations of the fluid and dust phase within the boundary layer, respectively.  $D_1$  and  $D_2$  are the coefficients of mass diffusivity of the fluid and dust particles, respectively.

The boundary conditions are:

$$\left. \begin{aligned} &\text{At } y = 0 : \\ &u = U_w = cx, v = v_w(x), T = T_w = T_\infty + A \left(\frac{x}{l}\right)^2, \\ &C = C_w = C_\infty + B \left(\frac{x}{l}\right)^2, C_p = C_{pw} = C_{p\infty} + E \left(\frac{x}{l}\right)^2 \\ &\text{As } y \rightarrow \infty : \\ &u \rightarrow 0, u_p \rightarrow 0, v_p \rightarrow v, \rho_p \rightarrow \omega\rho, \\ &T \rightarrow T_\infty, T_p \rightarrow T_\infty, C \rightarrow C_\infty, C_p \rightarrow C_{p\infty} \end{aligned} \right\} \quad (2.10)$$

where  $c > 0$  is the stretching rate,  $v_w(x)$  represents the permeability of the porous surface, and  $\omega$  is the density ratio. A, B, and E are positive constants and  $l = \sqrt{\frac{v_\infty}{c}}$  is the characteristic length.  $C_{pw}$  and  $C_{p\infty}$  are the species concentrations of dust particles at the surface of the plate and sufficiently far away from the flat surface, respectively.

### 3. Method of solution

To convert the governing equations into a set of similarity equations, we introduce the following transformations:

$$\left. \begin{aligned} &u = cx f'(\eta), v = -\sqrt{v_\infty} c f(\eta), \eta = \sqrt{\frac{c}{v_\infty}} y, \\ &u_p = cx F(\eta), v_p = \sqrt{c v_\infty} G(\eta), \rho_r = H(\eta), \\ &\theta(\eta) = \frac{T - T_\infty}{T_w - T_\infty}, \theta_p(\eta) = \frac{T_p - T_\infty}{T_w - T_\infty} \text{ where } T - T_\infty = A \left(\frac{x}{l}\right)^2 \theta(\eta), \\ &\phi(\eta) = \frac{C - C_\infty}{C_w - C_\infty} \text{ where } C - C_\infty = B \left(\frac{x}{l}\right)^2 \phi(\eta), \\ &\phi_p(\eta) = \frac{C_p - C_{p\infty}}{C_{pw} - C_{p\infty}} \text{ where } C_p - C_{p\infty} = E \left(\frac{x}{l}\right)^2 \phi_p(\eta). \end{aligned} \right\} \quad (3.1)$$

where  $v_\infty$  is the kinematic viscosity of the fluid in the free stream, and  $\rho_r = \frac{\rho_p}{\rho}$  is the relative density. The prime ( $'$ ) denotes the derivative with respect to  $\eta$ .

The viscosity of the fluid is assumed to be an inverse linear function of temperature, and it can be expressed, following Lai and Kulacki [14], in this way:

$$\frac{1}{\mu} = \frac{1}{\mu_\infty} [1 + \delta (T - T_\infty)] \quad (3.2)$$

$$\text{or, } \frac{1}{\mu} = \alpha (T - T_r),$$

where  $\alpha = \frac{\delta}{\mu_\infty}$  and  $T_r = T_\infty - \frac{1}{\delta}$ .

Moreover, the thermal conductivity of the fluid varies with temperature. Following Choudhury and Hazarika [15], we assumed the thermal conductivity of the fluid as:

$$\frac{1}{\lambda} = \frac{1}{\lambda_\infty} [1 + \xi (T - T_\infty)] \quad (3.3)$$

$$\text{or, } \frac{1}{\lambda} = \zeta (T - T_c),$$

where  $\zeta = \frac{\xi}{\lambda_\infty}$  and  $T_c = T_\infty - \frac{1}{\xi}$ .

Here,  $\alpha$ ,  $\delta$ ,  $\xi$ ,  $\zeta$ ,  $T_r$  and  $T_c$  are constants and their values depend on the reference state and thermal properties of the fluid, i.e.  $\nu$  (kinematic viscosity) and  $\lambda$  (thermal conductivity).  $\mu_\infty$  and  $\lambda_\infty$  are the viscosity and thermal conductivity of the ambient fluid.

Let us introduce two dimensionless parameters:

$\theta_r = \frac{T_r - T_\infty}{T_w - T_\infty}$  is the dimensionless reference temperature corresponding to viscosity, called the viscosity variation parameter, and  $\theta_c = \frac{T_c - T_\infty}{T_w - T_\infty}$  is the dimensionless reference temperature corresponding to thermal conductivity, called the thermal conductivity variation parameter. It is also important to note that  $\theta_r$  and  $\theta_c$  are negative for liquids and positive for gases [16].

Using these two parameters in Eqs. (3.2) and (3.3), we can write the coefficient of viscosity and thermal conductivity as follows:

$$\mu = -\frac{\mu_\infty \theta_r}{\theta - \theta_r} \quad \text{and} \quad \lambda = -\frac{\lambda_\infty \theta_c}{\theta - \theta_c} \quad (3.4)$$

Substituting Eqs. (3.1)–(3.4) in (2.2)–(2.9), we get:

$$\frac{\theta_r}{\theta - \theta_r} f''' - \frac{\theta_r}{(\theta - \theta_r)^2} \theta' f'' - f f'' + f'^2 + \frac{Fs}{Da} f'^2 - l^* \beta H (F - f') + M f'$$

$$- \frac{1}{Da Re} \frac{\theta_r}{\theta - \theta_r} f' - Gr \theta = 0 \quad (3.5)$$

$$GF' + F^2 + \beta (F - f') = 0 \quad (3.6)$$

$$GG' + \beta (f + G) = 0 \quad (3.7)$$

$$G^2 H' - \beta H(f + G) + GFH = 0 \quad (3.8)$$

$$\begin{aligned} \frac{\theta_c}{\theta - \theta_c} \theta'' - \frac{\theta_c}{(\theta - \theta_c)^2} \theta'^2 + \text{Pr}(2f'\theta - f\theta') - \frac{N}{\rho c \tau_T} \text{Pr}(\theta_p - \theta) - \frac{N}{\rho c \tau_v} \text{Pr} Ec(F - f')^2 \\ - \text{Pr} Q\theta - \frac{\theta_r}{\theta - \theta_r} \text{Pr} Ec f'^2 - \text{Pr} Ec M f'^2 = 0 \end{aligned} \quad (3.9)$$

$$G\theta'_p + 2F\theta_p + \frac{c_p}{cc_m \tau_T} (\theta_p - \theta) = 0 \quad (3.10)$$

$$\frac{\theta_r}{\theta - \theta_r} \phi'' - \frac{\theta_r}{(\theta - \theta_r)^2} \theta' \phi' + Sc(2f'\phi - f\phi') = 0 \quad (3.11)$$

$$\frac{\theta_r}{\theta - \theta_r} \phi''_p - \frac{\theta_r}{(\theta - \theta_r)^2} \theta' \phi'_p + Sc_p(2F\phi_p + G\phi'_p) = 0 \quad (3.12)$$

where the dimensionless parameters are defined as follows:

$l^* = mN/\rho$  is the mass concentration,

$\tau = m/K$  is the relaxation time of particle phase,

$\beta = l/c\tau$  is the fluid particle interaction parameter,

$\rho_r = \rho_p/\rho$  is the relative density,

$Gr = \frac{g\beta^*(T_w - T_\infty)}{c^2 x}$  is the Grashof number,

$M = \frac{\sigma B_0^2}{\rho c}$  is the magnetic field parameter,

$Da = \frac{k}{x^2}$  is the Darcy number,

$Re = \frac{u_w(x)x}{v_\infty}$  is the Reynolds number,

$Fs = \frac{c}{x}$  is the Forchhemier number,

$\text{Pr} = \frac{\mu_\infty c_p}{\lambda_\infty}$  is the Prandtl number,

$Ec = \frac{u_0^2}{c_p(T_w - T_\infty)}$  is the Eckert number,

$Q = \frac{Q_0}{c\rho c_p}$  is the heat generating parameter,

$Sc = \frac{\nu}{Dm}$  is the Schmidt number.

The boundary conditions (2.10) are reduced to:

$$\left. \begin{aligned} f = f_w, \quad f' = 1, \quad \theta = 1, \quad \phi = 1, \quad \phi_p = 1 \quad \text{at} \quad \eta = 0 \\ f' = 0, \quad F = 0, \quad G = -f, \quad H = \omega, \quad \theta = 0, \quad \theta_p = 0, \quad \phi = 0, \quad \phi_p = 0 \quad \text{as} \quad \eta \rightarrow \infty \end{aligned} \right\} \quad (3.13)$$

Governing Eqs. (3.5)–(3.13) are solved numerically using the fourth order Runge–Kutta method with the shooting technique.

The skin friction coefficient ( $C_f$ ), Nusselt number ( $Nu$ ), and Sherwood number ( $Sh$ ) are the parameters of physical and engineering interest, defined as follows:

The skin friction coefficient is defined as:

$$C_f = \frac{2\tau_w}{\rho_\infty u_0^2}, \text{ where } \tau_w = \mu \left. \frac{\partial u}{\partial y} \right)_{y=0} \text{ is the shearing stress.}$$

Using the nondimensional variables, we finally get the skin friction coefficient as:

$$C_f = -\frac{2\theta_r}{1-\theta_r} Re^{-1/2} f''(0).$$

The local Nusselt number is defined as:

$$Nu = \frac{-xq_w}{\lambda_\infty(T_w - T_\infty)}, \text{ where } q_w = -\lambda \left. \frac{\partial T}{\partial y} \right)_{y=0} \text{ is the heat transfer from the sheet.}$$

Using the nondimensional variables, we get:

$$Nu = \frac{\theta_c}{1-\theta_c} Re^{1/2} \theta'(0).$$

The local Sherwood number is defined as:

$$Sh = \frac{xm_w}{Dm_\infty(C_w - C_\infty)}, \text{ where } m_w = -Dm \left. \frac{\partial C}{\partial y} \right)_{y=0} \text{ is the mass flux at the surface and } Dm_\infty \text{ is the}$$

diffusion coefficient at free stream.

Using the nondimensional variables we get the following:

$$Sh = -Re^{-1/2} Sc^{-1} \frac{\theta_r}{1-\theta_r} \phi'(0).$$

#### 4. Results and discussion

The boundary value problem (3.5–3.13) was solved using the fourth order Runge–Kutta shooting method. Computations were carried out for different values of the viscosity variation parameter ( $\theta_r$ ), thermal conductivity variation parameter ( $\theta_c$ ), magnetic parameter ( $M$ ), Eckert number ( $Ec$ ), Prandtl number ( $Pr$ ), heat generating parameter ( $Q$ ), fluid particle interaction parameter ( $\beta$ ), and the number density of dust particles ( $N$ ), i.e. the number of dust particles per unit volume of the mixture. Results are presented through graphs for velocity  $f'(\eta)$  and  $F(\eta)$ , temperature  $\theta(\eta)$  and  $\Theta_p(\eta)$ , and species concentration  $\phi(\eta)$  and  $\Phi_p(\eta)$  in Figures 2–22. The values of the parameters are taken as:  $f_w=1$ ,  $\lambda=0.5$ ,  $Q=0.75$ ,  $Re=10$ ,  $Fs=0.1$ ,  $Da=1.5$ ,  $Gm = Gr = 0.5$ ,  $M = 1$ ,  $Pr = 0.71$ ,  $Sc = Sc_p = 0.22$ ,  $l^* = 0.2$ ,  $\beta = 0.5$ ,  $N = 0.5$ ,  $\rho = 1$ ,  $c = 0.6$ ,  $\tau_T = 0.5$ ,  $\tau_v = 1$ ,  $\omega = 0.1$ ,  $Ec = 0.05$ ,  $c_p = c_m = 0.2$ ,  $\theta_r = 5$ , and  $\theta_c = 3$ , unless stated otherwise.

Figures 2–4 show the effect of  $\theta_r$  and Figures 5–7 present the effect of  $\theta_c$  on velocities  $f'$  and  $F$ , temperatures  $\Theta$  and  $\Theta_p$ , and species concentrations  $\phi$  and  $\phi_p$ , respectively. From Figures 2–4 it is seen that for increasing values of the viscosity variation parameter  $\theta_r$ , velocity, and species concentration decrease for both the fluid and dust phases, whereas temperature increases. This is expected because in a gas, viscosity increases with increasing temperature. Figures 5–7 show that an increase in the thermal conductivity variation parameter  $\theta_c$  leads to increases in the velocity and species concentration profiles for both the fluid and dust phases, while the opposite happens with the temperature profiles for both phases. This is expected because thermal conductivity is an inverse linear function of temperature.

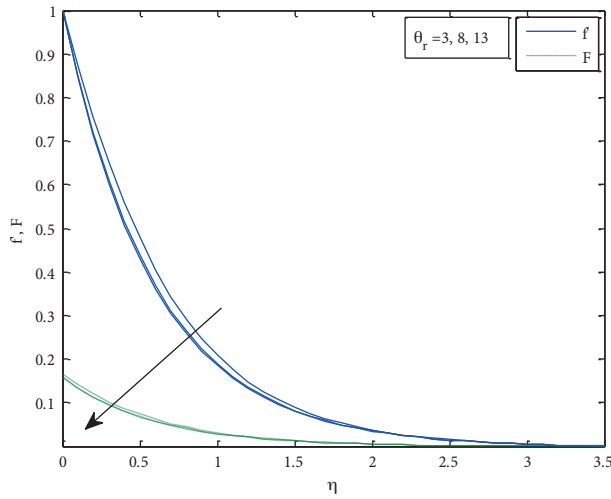


**Figure 2.** Velocity profile for different  $\Theta_r$ .

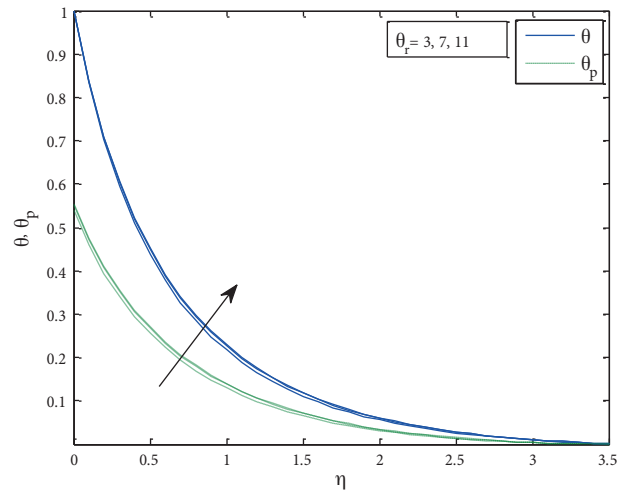


**Figure 3.** Temperature profile for different  $\Theta_r$ .

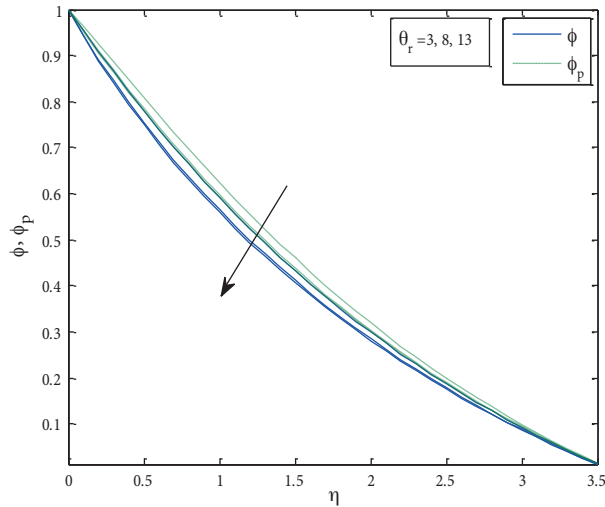


**Figure 4.** Concentration profile for different  $\Theta_r$ .

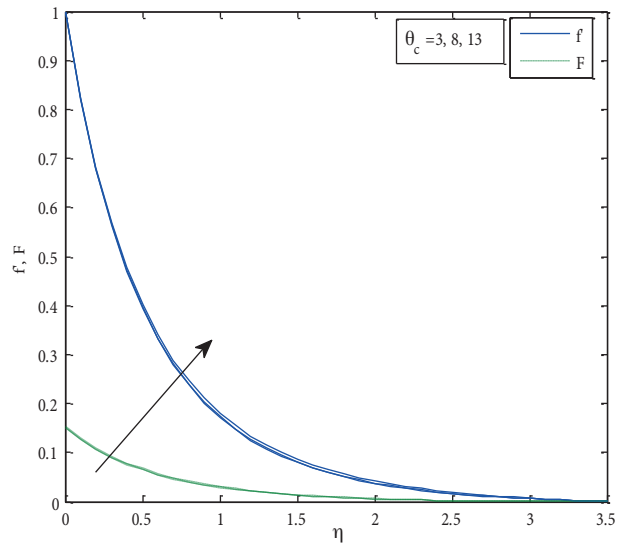


**Figure 5.** Velocity profile for different  $\Theta_c$ .

Velocity profiles, temperature profiles, and concentration profiles for different values of the magnetic parameter  $M$  are presented in Figures 8–10. Figure 8 shows that fluid velocity considerably decreased with the increasing values of  $M$  due to the effect of Lorentz force, for which one resistive term appears in the momentum equations and a Joule dissipation term appears in the energy equation. Clearly the transverse magnetic field opposes fluid velocity. Notice that the velocity of the dust particle phase also decreases with increasing values of  $M$ , although solid particles are electrically nonconductive. This is expected because fluid velocity is the source of dust particle velocity. Figure 9 depicts the temperature profiles for different values of the magnetic parameter  $M$ . Analysis of the graph shows that the effect of increasing values of  $M$  is to enhance the temperature, tending asymptotically to zero as the distance increases from the boundary for both the fluid and dust phases. This is due to the fact that Joule dissipation increases as magnetic parameter  $M$  increases. We infer from Figure 10 that species concentration increases with increasing values of  $M$ .

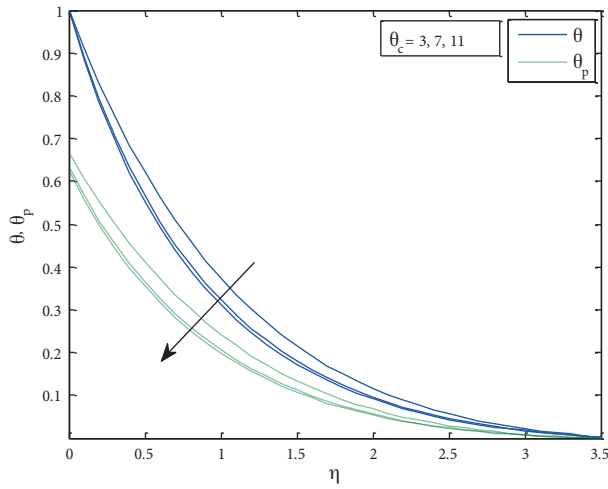


Figure 6. Temperature profile for different  $\Theta_c$ .

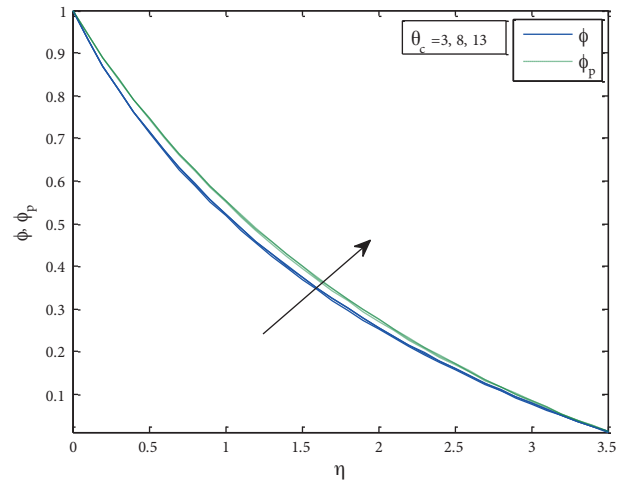


Figure 7. Concentration profile for different  $\Theta_c$ .

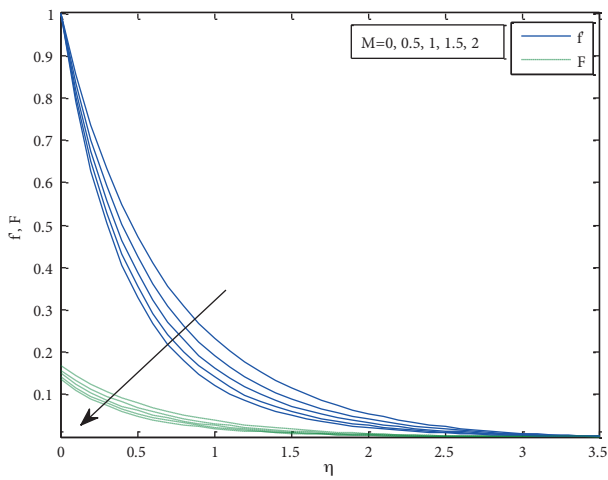


Figure 8. Velocity profile for different  $M$ .

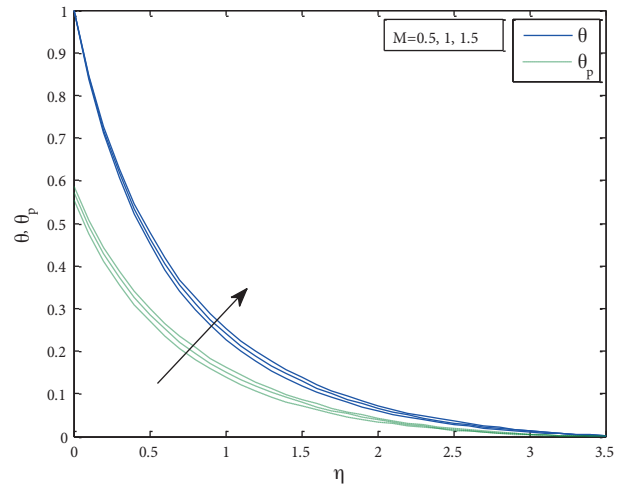


Figure 9. Temperature profile for different  $M$ .

Figures 11–13 indicate the effect of the Prandtl number  $Pr$  on velocities  $f'$  and  $F$ , temperatures  $\Theta$  and  $\Theta_p$ , and species concentrations  $\phi$  and  $\phi_p$ , respectively. Since  $Pr$  is the ratio of boundary layer velocity to thermal boundary layer velocity, boundary layer velocity and thermal boundary layer velocity coincide when  $Pr = 1$ . When  $Pr < 1$ , it means that heat diffuses very quickly compared with velocity, hence velocity and temperature decrease with the increase of  $Pr$ , but species concentration increases under the same condition.

Velocity, temperature, and species concentration profiles for different values of heat generating parameter  $Q$  are plotted for both the fluid and dust phase in Figures 14–16. It is observed from Figure 14 that velocity profiles increase with the increase of the heat generating parameter  $Q$ . It is due to the fact that when heat is generated, the buoyancy force increases, which induces the flow rate to increase, giving rise to an increase in the velocity profiles for both fluid and dust phases. From Figure 15 it is seen that when the value of the heat generation parameter  $Q$  increases, the temperature distribution also increases significantly, while species concentration decreases.

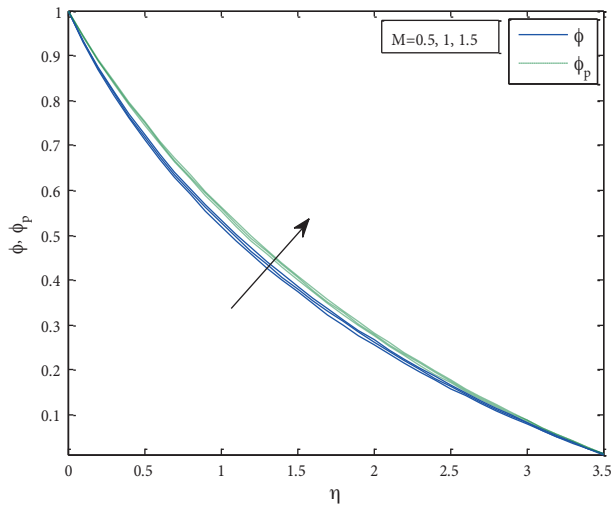


Figure 10. Concentration profile for different  $M$ .

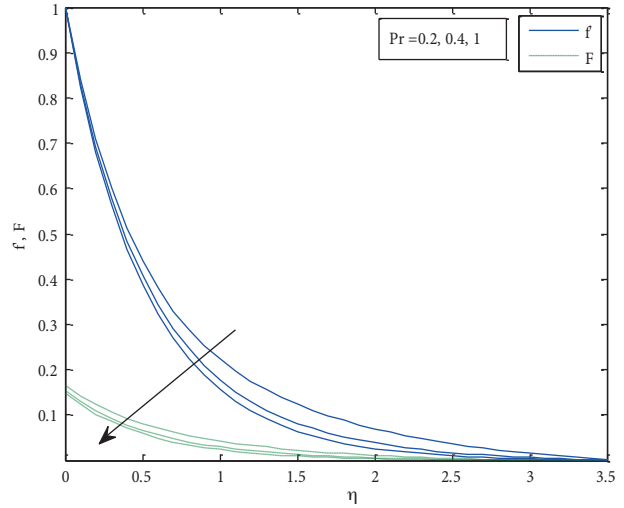


Figure 11. Velocity profile for different  $Pr$ .

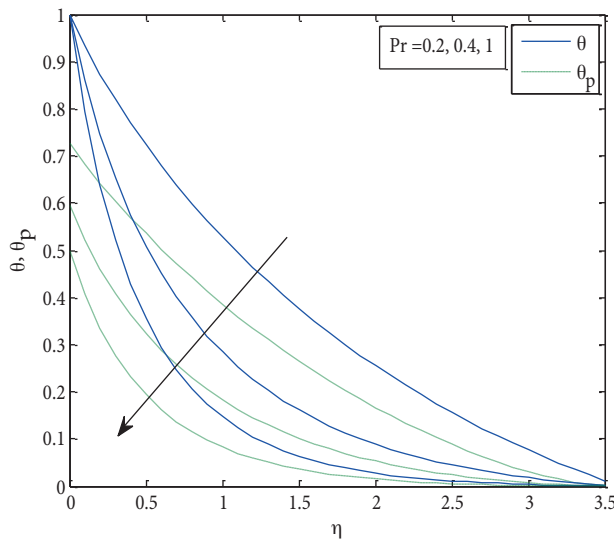


Figure 12. Temperature profile for different  $Pr$ .

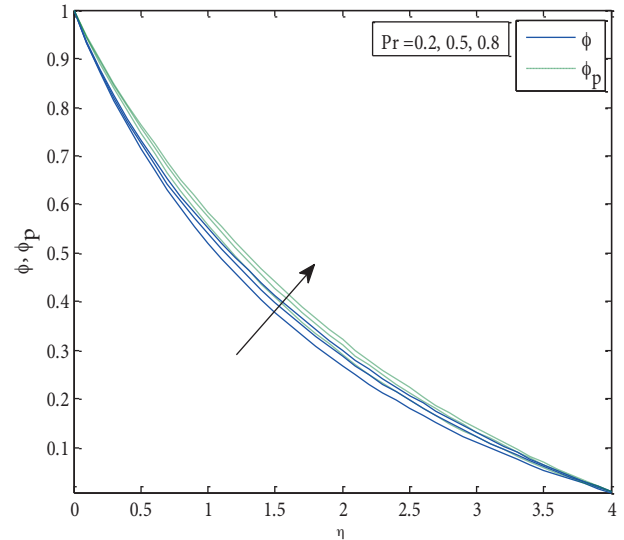


Figure 13. Concentration profile for different  $Pr$ .

Figures 17–19 illustrate the variations of velocity, temperature, and species concentration profiles for various values of the fluid particle interaction parameter  $\beta$ . It is clearly observed from these figures that velocity increases with the increase of  $\beta$ , but temperature and species concentration profiles decrease for both the fluid and dust phases.

Figures 20–22 depict the velocity, temperature, and species concentration profiles for different values of the number density parameter  $N$ . As  $N$  increases, velocity and temperature profiles for both the fluid and dust phases decrease, while species concentration increases.

Tables 1–10 demonstrate the effects of various parameters on the skin friction coefficient  $C_f$ , representing plate shearing stress, the rate of heat transfer from the plate to the fluid in terms of the Nusselt number  $Nu$ , and the rate of mass transfer in terms of the Sherwood number  $Sh$ .

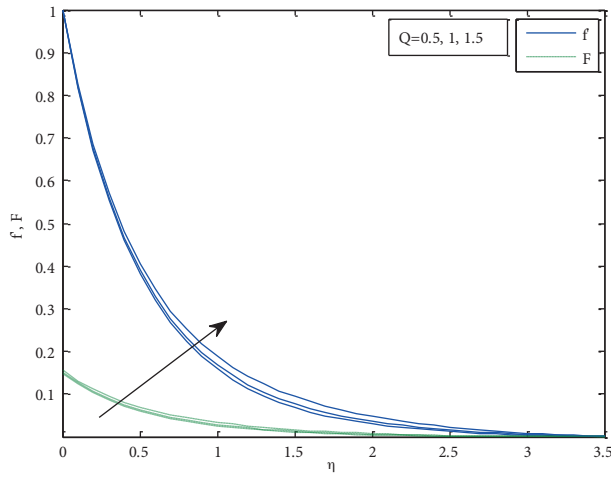


Figure 14. Velocity profile for different  $Q$ .

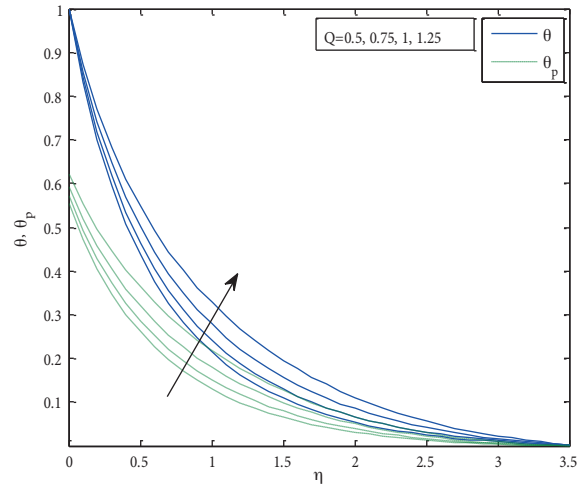


Figure 15. Temperature profile for different  $Q$ .

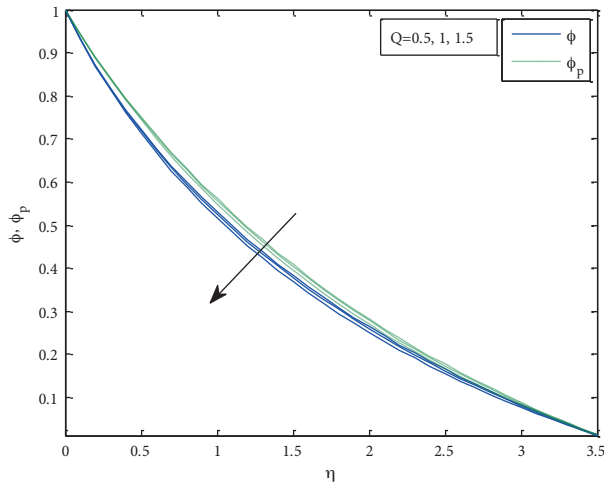


Figure 16. Concentration profile for different  $Q$ .

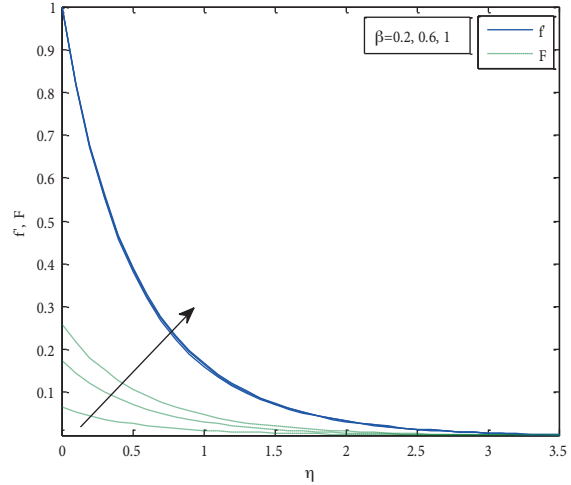


Figure 17. Velocity profile for different  $\beta$ .

Table 1. Effects of  $\Theta_r$  and  $M$  on the local skin friction coefficient ( $C_f$ ), local Nusselt number ( $Nu$ ), and local Sherwood number ( $Sh$ ).

$M \rightarrow$	0.5			1			1.5			
	$\Theta_r \downarrow$	$C_f$	$Nu$	$Sh$	$C_f$	$Nu$	$Sh$	$C_f$	$Nu$	$Sh$
3		-0.34795	19.24611	-0.33524	-0.39123	18.84529	-0.32963	-0.43035	18.49486	-0.32493
5		-0.33546	18.98571	-0.32436	-0.37622	18.56517	-0.31871	-0.41291	18.19926	-0.31399
7		-0.33053	18.87846	-0.31996	-0.37032	18.45021	-0.3143	-0.40607	18.07834	-0.30958
9		-0.32789	18.81997	-0.31757	-0.36716	18.38761	-0.31191	-0.40242	18.01259	-0.3072

From these tables it is observed that the skin friction coefficient  $C_f$  decreases with increasing values of the thermal conductivity parameter  $\theta_c$ , the magnetic parameter  $M$ , Prandtl number  $Pr$ , Eckert number  $Ec$ , and the number density parameter  $N$ . However, it increases with the increase of the viscosity parameter  $\theta_r$  and the fluid particle interaction parameter  $\beta$ . Physically negative values of  $C_f$  mean that the surface exerts a drag force on the fluid so that stretching the surface will induce the flow.

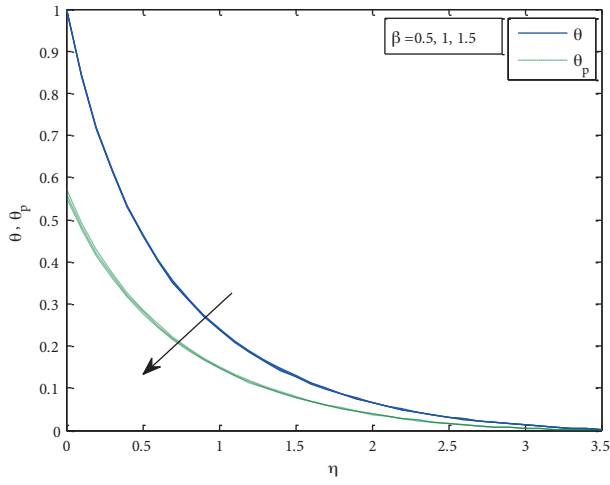


Figure 18. Temperature profile for different  $\beta$ .

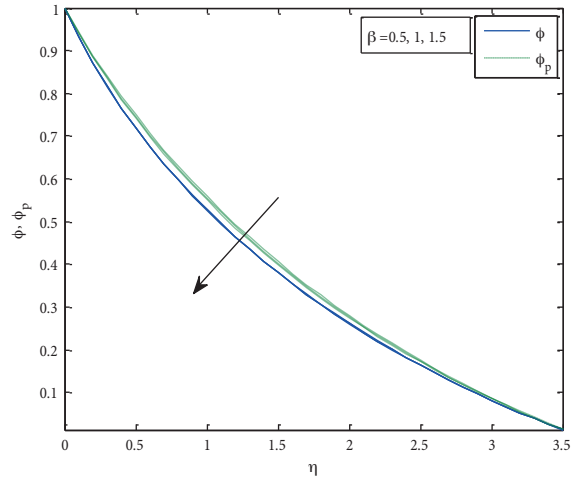


Figure 19. Concentration profile for different  $\beta$ .

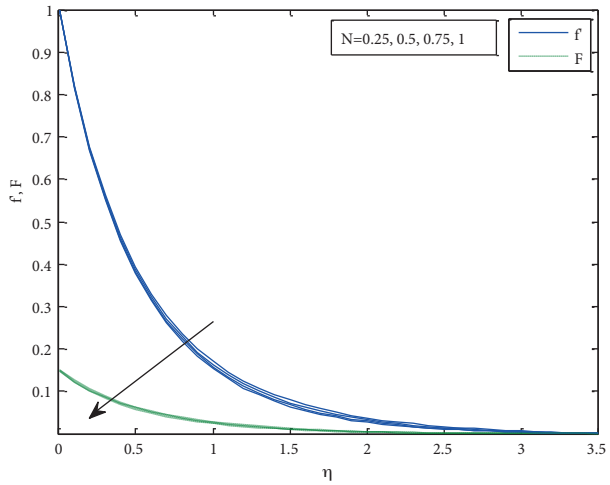


Figure 20. Velocity profile for different  $N$ .

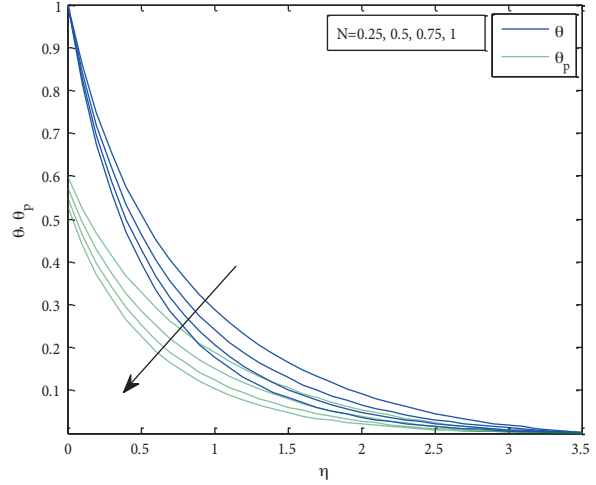


Figure 21. Temperature profile for different  $N$ .

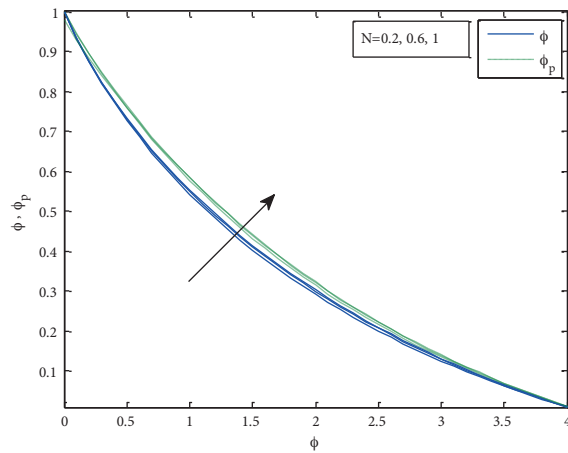


Figure 22. Concentration profile for different  $N$ .

**Table 2.** Effects of  $\Theta_c$  and  $M$  on the local skin friction coefficient ( $C_f$ ), local Nusselt number ( $Nu$ ), and local Sherwood number ( $Sh$ ).

M→	0.5			1			1.5		
$\Theta_c \downarrow$	$C_f$	Nu	Sh	$C_f$	Nu	Sh	$C_f$	Nu	Sh
3	-0.29267	9.960165	-0.29685	-0.32835	9.626789	-0.29103	-0.36016	9.341308	-0.2862
5	-0.29599	11.69225	-0.29667	-0.33144	11.32562	-0.29091	-0.36306	11.01147	-0.28613
7	-0.29725	12.42242	-0.29661	-0.33262	12.04286	-0.29087	-0.36417	11.71753	-0.28611
9	-0.29791	12.82519	-0.29658	-0.33325	12.43874	-0.29085	-0.36476	12.10746	-0.2861

**Table 3.** Effects of  $\Theta_r$  and  $Pr$  on the local skin friction coefficient ( $C_f$ ), local Nusselt number ( $Nu$ ), and local Sherwood number ( $Sh$ ).

Pr→	0.5			0.75			1.5		
$\Theta_r \downarrow$	$C_f$	Nu	Sh	$C_f$	Nu	Sh	$C_f$	Nu	Sh
3	-0.38752	14.35384	-0.33577	-0.3918	19.69002	-0.32866	-0.39462	24.86341	-0.32371
5	-0.371	14.10388	-0.32299	-0.37706	19.40703	-0.31803	-0.38131	24.57536	-0.31454
7	-0.36457	14.00264	-0.31789	-0.37124	19.29067	-0.31373	-0.37602	24.45582	-0.31081
9	-0.36116	13.94785	-0.31514	-0.36813	19.22723	-0.3114	-0.37317	24.39038	-0.30879

**Table 4.** Effects of  $\Theta_c$  and  $Pr$  on the local skin friction coefficient ( $C_f$ ), local Nusselt number ( $Nu$ ), and local Sherwood number ( $Sh$ ).

Pr→	0.5			0.75			1.5		
$\Theta_c \downarrow$	$C_f$	Nu	Sh	$C_f$	Nu	Sh	$C_f$	Nu	Sh
3	-0.32088	7.376718	-0.29174	-0.32967	10.06401	-0.29092	-0.33715	12.8127	-0.29039
5	-0.32384	8.639446	-0.29154	-0.33277	11.84469	-0.29081	-0.34016	15.09175	-0.29039
7	-0.32498	9.172213	-0.29147	-0.33395	12.59642	-0.29078	-0.34129	16.05322	-0.29039
9	-0.32559	9.46623	-0.29143	-0.33458	13.01133	-0.29077	-0.34189	16.58377	-0.2904

**Table 5.** Effects of  $\Theta_r$  and  $Ec$  on the local skin friction coefficient ( $C_f$ ), local Nusselt number ( $Nu$ ), and local Sherwood number ( $Sh$ ).

Ec→	0.1			0.03			0.5		
$\Theta_r \downarrow$	$C_f$	Nu	Sh	$C_f$	Nu	Sh	$C_f$	Nu	Sh
3	-0.39117	18.7102	-0.32974	-0.3912	18.77769	-0.32969	-0.39123	18.84528	-0.32963
5	-0.37614	18.42556	-0.31878	-0.37618	18.49531	-0.31874	-0.37622	18.56517	-0.31871
7	-0.37022	18.30914	-0.31436	-0.37027	18.37964	-0.31433	-0.37032	18.45022	-0.3143
9	-0.36706	18.24584	-0.31196	-0.36711	18.31667	-0.31194	-0.36716	18.38761	-0.31191

**Table 6.** Effects of  $\Theta_c$  and  $Ec$  on the local skin friction coefficient ( $C_f$ ), local Nusselt number ( $Nu$ ), and local Sherwood number ( $Sh$ ).

Ec→	0.1			0.03			0.5		
$\Theta_c \downarrow$	$C_f$	Nu	Sh	$C_f$	Nu	Sh	$C_f$	Nu	Sh
3	-0.32826	9.563625	-0.29103	-0.32831	9.595186	-0.29103	-0.32835	9.626787	-0.29103
5	-0.33135	11.24658	-0.29091	-0.33139	11.28608	-0.29091	-0.33144	11.32563	-0.29091
7	-0.33253	11.95688	-0.29087	-0.33258	11.99984	-0.29087	-0.33262	12.04285	-0.29087
9	-0.33315	12.3489	-0.29085	-0.3332	12.39379	-0.29085	-0.33325	12.43874	-0.29085

**Table 7.** Effects of  $\Theta_r$  and  $N$  on the local skin friction coefficient ( $C_f$ ), local Nusselt number ( $Nu$ ), and local Sherwood number ( $Sh$ ).

$N \rightarrow$	1			2			3		
$\Theta_r \downarrow$	$C_f$	$Nu$	$Sh$	$C_f$	$Nu$	$Sh$	$C_f$	$Nu$	$Sh$
3	-0.39123	18.84528	-0.32963	-0.39344	21.98691	-0.32596	-0.39493	24.78926	-0.32336
5	-0.37622	18.56517	-0.31871	-0.37947	21.74391	-0.31607	-0.38175	24.57331	-0.31422
7	-0.37032	18.45022	-0.3143	-0.37395	21.64374	-0.31207	-0.37652	24.48393	-0.31051
9	-0.36716	18.38761	-0.31191	-0.37099	21.58905	-0.3099	-0.37372	24.4351	-0.3085

**Table 8.** Effects of  $\Theta_c$  and  $N$  on the local skin friction coefficient ( $C_f$ ), local Nusselt number ( $Nu$ ), and local Sherwood number ( $Sh$ ).

$N \rightarrow$	1			2			3		
$\Theta_c \downarrow$	$C_f$	$Nu$	$Sh$	$C_f$	$Nu$	$Sh$	$C_f$	$Nu$	$Sh$
3	-0.32835	9.626787	-0.29103	-0.33447	11.60301	-0.29054	-0.3391	13.38001	-0.29026
5	-0.33144	11.32563	-0.29091	-0.33739	13.59309	-0.2905	-0.34184	15.6223	-0.29028
7	-0.33262	12.04285	-0.29087	-0.3385	14.42914	-0.29049	-0.34288	16.56118	-0.2903
9	-0.33325	12.43874	-0.29085	-0.33908	14.88963	-0.29049	-0.34342	17.07757	-0.29031

**Table 9.** Effects of  $\Theta_r$  and  $\beta$  on the local skin friction coefficient ( $C_f$ ), local Nusselt number ( $Nu$ ), and local Sherwood number ( $Sh$ ).

$\beta \rightarrow$	0.5			1			1.5		
$\Theta_r \downarrow$	$C_f$	$Nu$	$Sh$	$C_f$	$Nu$	$Sh$	$C_f$	$Nu$	$Sh$
3	-0.39123	18.84528	-0.32963	-0.38491	18.95267	-0.33043	-0.38034	19.03179	-0.33105
5	-0.37622	18.56517	-0.31871	-0.37037	18.67429	-0.31951	-0.36612	18.75484	-0.32012
7	-0.37032	18.45022	-0.3143	-0.36464	18.55994	-0.3151	-0.36051	18.641	-0.31571
9	-0.36716	18.38761	-0.31191	-0.36158	18.49763	-0.31271	-0.35751	18.57896	-0.31332

**Table 10.** Effects of  $\Theta_c$  and  $\beta$  on the local skin friction coefficient ( $C_f$ ), local Nusselt number ( $Nu$ ), and local Sherwood number ( $Sh$ ).

$\beta \rightarrow$	0.5			1			1.5		
$\Theta_c \downarrow$	$C_f$	$Nu$	$Sh$	$C_f$	$Nu$	$Sh$	$C_f$	$Nu$	$Sh$
3	-0.32835	9.626787	-0.29103	-0.32345	9.710939	-0.29183	-0.3199	9.773203	-0.29243
5	-0.33144	11.32563	-0.29091	-0.32657	11.4169	-0.2917	-0.32301	11.48452	-0.2923
7	-0.33262	12.04285	-0.29087	-0.32775	12.13687	-0.29166	-0.3242	12.20654	-0.29225
9	-0.33325	12.43874	-0.29085	-0.32838	12.53421	-0.29164	-0.32482	12.60497	-0.29223

Furthermore, it is seen that the values of the Nusselt number ( $Nu$ ) increase with increasing values of the thermal conductivity parameter  $\theta_c$ , Prandtl number  $Pr$ , Eckert number  $Ec$ , the number density parameter  $N$ , and the fluid particle interaction parameter  $\beta$ , while it decreases with increases in the viscosity parameter  $\theta_r$  and magnetic parameter  $M$ .

From these tables we observed that the Sherwood number ( $Sh$ ) increases with the increasing values of the viscosity variation parameter  $\theta_r$ , thermal conductivity variation parameter  $\theta_c$ , magnetic parameter  $M$ , Prandtl number  $Pr$ , Eckert number  $Ec$ , and the number density parameter  $N$ . However, it decreases with increasing values of the fluid particle interaction parameter  $\beta$ .

## Conclusion

Based on the results of the present study, the following observations were made:

- (1) The motion of both the fluid and dust phase is retarded under the application of a transverse magnetic field due to Lorentz force.
- (2) The velocity of the fluid and dust phase decreases with increases in the viscosity variation parameter ( $\theta_r$ ), Prandtl number ( $Pr$ ), and the number density of the fluid particle ( $N$ ). However, it increases with increases in the thermal conductivity variation parameter ( $\theta_c$ ), fluid particle interaction parameter ( $\beta$ ), and heat generating parameter ( $Q$ ).
- (3) The temperature increases with increasing viscosity variation parameter ( $\theta_r$ ), heat generating parameter ( $Q$ ), and magnetic field, while it decreases as thermal conductivity,  $Pr$ ,  $\beta$ , and  $N$  increase.
- (4) Species concentration decreases with increasing values of the viscosity variation parameter ( $\theta_c$ ) and the heat generating parameter for both the fluid and dust phases.
- (5) The effect of increasing the thermal conductivity variation parameter ( $\theta_c$ ), the magnetic field,  $Pr$  and  $N$  is to increase the species concentration.
- (6) The velocity and temperature of the fluid phase are higher than those of the dust phase.
- (7) The wall shear stress of fluid decreases with increases in the thermal conductivity, viscosity, magnetic field, viscous dissipation, and the number density of dust particle.
- (8) The rate of heat transfer increases with increasing viscous dissipation, thermal conductivity, and  $Pr$ . However, it decreases with increasing values of viscosity and magnetic field.
- (9) The rate of mass transfer at the plate is considerably increased due to increasing viscosity, thermal conductivity, and magnetic field, while it decreases with increases in the fluid particle interaction parameter.

## 5. Nomenclature

$(u, v)$	are the velocity components of the fluid,
$(u_p, v_p)$	are the velocity components of dust phase,
$\rho$	is the density of the fluid,
$\mu$	is the coefficient of dynamic viscosity,
$\mu_\infty$	is the coefficient of dynamic viscosity of the ambient fluid,
$\nu_\infty$	is the kinematic viscosity of the fluid in the free stream,
$\rho_p$	is the density of the particle phase,
$N$	is the number density of the particle phase,
$K$	is the Stokes' resistance (drag coefficient),
$m$	is the mass of the dust particle,
$g$	is the acceleration due to gravity,
$\beta^*$	is the volumetric coefficient of thermal expansion,
$\beta^{**}$	is the volumetric coefficient of concentration expansion,
$T$	is the temperature of the fluid inside the boundary layer,
$T_\infty$	is the temperature of the fluid at free stream,
$T_p$	is the temperature of the dust particles inside the boundary layer,
$T_{p\infty}$	is the temperature of the dust particles in the free-stream,

$C_{pw}$ and $C_{p\infty}$	are the species concentration of dust particles at the surface of the plate and sufficiently far away from the flat surface respectively,
$\omega$	is the density ratio,
$\sigma$	is the electrical conductivity,
$c$	is the stretching rate,
$l$	is the characteristic length,
$c_p$	is the specific heat of fluid at constant pressure,
$c_m$	is the specific heat of dust particles at constant pressure,
$\tau_T$	is the thermal equilibrium time and is the time required by the dust cloud to adjust its temperature to the fluid,
$\tau_v$	is the relaxation time of the dust particle, i.e. the time required by a dust particle to adjust its velocity relative to the fluid,
$\lambda$	is the thermal conductivity of the fluid,
$\lambda_\infty$	is the thermal conductivity of the ambient fluid,
$C$	is the species concentration of the fluid,
$C_p$	is the concentration of the dust phase within the boundary layer,
$D_1$	is the coefficient of mass diffusivity of the fluid,
$D_2$	is the coefficient of mass diffusivity of dust phase,
$\theta_r$	is the viscosity variation parameter,
$\theta_c$	is the thermal conductivity variation parameter,
$l^*$	is the mass concentration,
$\tau$	is the relaxation time of particle phase,
$\beta$	is the fluid particle interaction parameter,
$Gr$	is the Grashof number,
$M$	is the magnetic field parameter,
$Da$	is the Darcy number,
$Re$	is the Reynolds number,
$Fs$	is the Forchhemier number,
$Pr$	is the Prandtl number,
$Ec$	is the Eckert number,
$Q$	is the heat generating parameter,
$Q_0$	is the volumetric rate of heat generation,
$Sc$	is the Schmidt number,
$C_f$	is the skin friction coefficient,
$Nu$	is the Nusselt number,
$Sh$	is the Sherwood number.

## References

- [1] Saffman, P. G. *J. Fluid Mec. A*, **1962**, *13*, 120–128.
- [2] Datta, N.; Mishra, S. K. *Acta Mech.*, **1982**, *42*, 71–83.
- [3] Asmolov E. S; Manuilovich S. V. *J. Fluid Mech.*, **1998**, *365*, 137-170.
- [4] Palani, G.; Ganesan, P. *Forsch. Ingenieurwes.*, **2007**, *71*, 223-230.
- [5] Agranat, V. M. *Fluid Dyn.*, **1988**, *23*, 729-732.
- [6] Vajravelu, K.; Nayfeh, J. *Int. J. Nonlinear Mech.*, **1992**, *27*, 937-945.
- [7] Gireesha, B. J.; Ramesh, G. K.; Abel, S.; Bagewadi, C. S. *Int J. Multiphas. Flow*, **2011**, *37*, 977–982.
- [8] Gireesha, B. J.; Ramesh, G. K.; Bagewadi, C. S. *Adv. Appl. Sci. Res.*, **2012**, *3*, 2392–2401.
- [9] Gireesha, B. J.; Ramesh, G. K.; Bagewadi, C. S. *Appl. Math. Mech.-Engl.*, **2012**, *33*, 1001–1014.

- [10] Kishan, N.; Deepa, G. *Adv. Appl. Sci. Res.*, **2012**, *3*, 430-439.
- [11] Gaikwad, S. N.; Rahuldev, B. M. *Adv. Appl. Sci. Res.*, **2012**, *3*, 720-734.
- [12] Hazarika, G. C. *Int. J. Comput. Appl. T.*, **2014**, *103*, 39-45.
- [13] Herwig, H.; Wicken, G. *Warme Stoffubertrag.*, **1986**, *20*, 47-57.
- [14] Lai, F. C.; Kulacki, F.A. *Int. J. Heat Mass Tran.*, **1991**, *33*, 1028-1031.
- [15] Choudhury, M.; Hazarika, G. C. *J. Appl. Fluid Mech.*, **2013**, *6*, 277-283.
- [16] Kuppalapalle, V.; Vinayaka, P. K.; Chiu-On, N. *J. Hydrodyn.*, **2013**, *25*, 1-9.